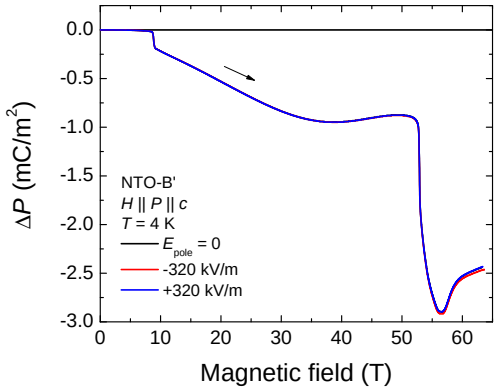

FIG. S1. Magnetic field-dependence of electric polarization of Ni_3TeO_6 under different poling electric field. Sample was poled with an applied electric field at zero magnetic field at 60 K and then cooled down to 4 K. Electric field was kept on ($\pm$320 kV/m) during the measurement. Virtually, no electric field dependence is observed demonstrating that NTO is pyroelectric, not ferroelectric.

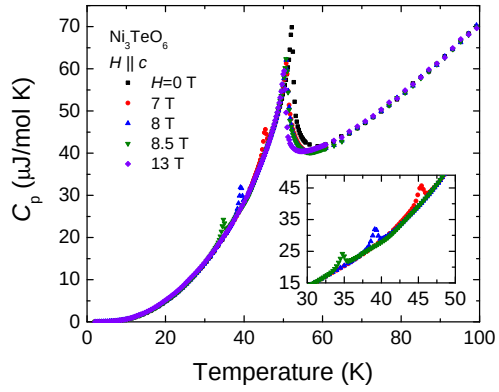

FIG. S2. Specific heat of Ni_3TeO_6 under different magnetic field applied along the c axis. Inset shows the enlarged view to show the SF transition.

Details of the experiment

Single crystals of Ni_3TeO_6 (NTO) were grown by chemical vapor transport method [1]. Magnetization (M) above 13 T was measured in a pulse magnet by recording the induced voltage in a triply-compensated coil [2] and calibrated by vibrating sample magnetometry measurements in a superconducting magnet (PPMS-14, Quantum Design). Magnetostriction ($\Delta L/L$) was measured up to 92 T along the c-axis using an optical fiber grating technique [3]. During the magnetostriction measurement, the ab-plane of the sample was attached to a platform for mechanical stabilization during the rapid magnetic field pulse. The absolute value of magnetostriction was checked and calibrated against a capacitive dilatometer measurement in a superconducting magnet up to 13 T [4]. Hexagonal shaped platelet-like crystals (typically 0.5 mm^2 in area and 90 μm thick) were used for dielectric constant (ε) and P measurements along the c-axis. Electric polarization was obtained under pulsed-field conditions by measuring the magnetoelectric current and integrating it over time [5, 6]. Prior to the measurement, samples were poled by cooling from 75 K to measurement temperature in a static poling electric field (E_{pole}) up to 320 kV/m. However, we find no E_{pole}-dependence of P in our measurements as shown in Fig. S1. High magnetic fields were generated using either a capacitor-driven pulse magnet up to 65 T or a hybrid pulse magnet (combination of generator- and capacitor-driven magnets) up to 92 T at NHMFL in Los Alamos. Specific heat was measured by using a relaxation method in a PPMS-14 (Fig. S2).

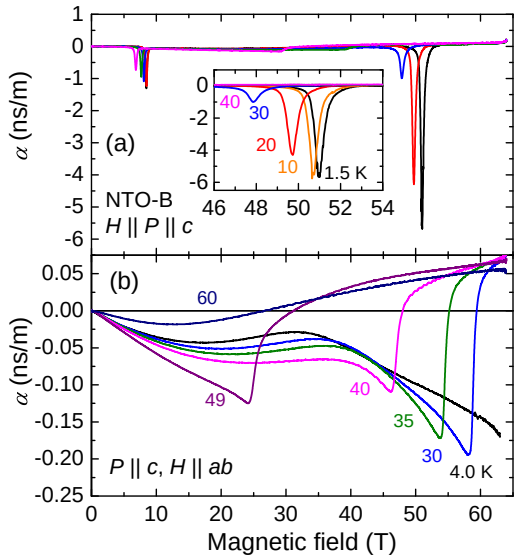

FIG. S3. Magnetoelectric coefficient α as a function of magnetic field for (a) $H\|c$ and (b) $H\|ab$. Inset in (a) shows a expanded plot of α at the high-field transition.

Linear magnetoelectric coefficient

To visualize the giant response of P to the external magnetic field, we plot the ME coefficient $\alpha(\equiv \mathrm{d}P/\mathrm{d}H)$ of NTO as a function of magnetic field (Fig. S3). In the case of c-axis magnetic field, one can immediately see that the ME coefficient value at H_{c2} is almost four times greater than that at H_{c1} (Fig. S3(a)) and reaches up to 6,000 ps/m which is one of very high α value observed among the ME materials to date [7–9].

Details of the first-principles calculations

In order to model the magnetism in NTO it is essential to know the exchange constants. They were calculated using DFT previously [10], but, unfortunately, the minimization of the energy Eq. 1 of the main text within the 6-atom magnetic unit cell using those values gives a non-collinear state at a moderate K_2, while experiments suggest a collinear ground state [11]. We have found that the collinear state could be stabilized by reducing the exchange constant J_5 by 30%. Since Ni ions are centered in similar oxygen octahedra, we assumed the anisotropy constants to be equal, $K_{2,i} = K_2$, and chose their value to match the spin flop field measured experimentally. The calculated $M(H)$ curve is very different from the experimentally observed one - the magnetization jump at the spin flop transition is overestimated, and the second transition is absent. In order to improve the model we calculated the exchange constants using the PBE0 hybrid density functional, which is known to give better estimates for exchange constants in some compounds [12]. We used the VASP code with the supplied PAW-PBE atomic files [13–20], with the plane wave cutoff of 500 eV; spin-orbit coupling was neglected; energy convergence threshold was set to 10^{-6} eV; total energy was evaluated using Γ-centered $4 \times 4 \times 4$ k-point grid. The PBE0 calculation was seeded with the wavefunctions, calculated using PBE+U with $U = 8$ eV applied on Ni d-orbitals. The PBE0 total energies for 10 different spin arrangements within the magnetic unit cell were fitted to the model Eq. 1 of the main text using a least-square fit. The choice of trial magnetic states ensured that the system is overdetermined. The relative error for $J_1 \dots J_4$ was estimated below 12 %, for J_5 – 37 %. Fig. S5 compares the energies of the used spin states, calculated using PBE0 [21] and from the fit.

The obtained exchange constants result in the experimentally observed ground state and the appearance of the second transition without any additional tuning, as shown in Fig. S6. The critical field H_{c2} of the second transition is not sensitive to K_2. The magnetization change at H_{c2} is much smaller than that observed in the experiment. Starting from these values, we tuned the exchange constants to improve the agreement between the calculated and measured M along the c-axis. The final result is presented on Fig. 2(g), and the values of exchange constants are summarized in Table 1 of the main text.

Due to a frustration in NTO the ground state could be sensitive to small variations of exchange constants, therefore hybrid functional calculations were required to reproduce the correct ground state. However, these calculations are computationally expensive, therefore we used a faster GGA + U as implemented in VASP to estimate the polarization variations in response to changes of spin arrangement, encoded in α_n. Hubbard U = 4.5 eV was applied to Ni d orbitals in these calculations. The 20-atom rhombohedral unit cell, containing 2 formula units, were relaxed with the magnetic moments of Ni initialized to be in 10 trial configurations, and we have checked that the directions of magnetic moments didn't change during the procedure. Total energies and Berry-phase polarizations were then calculated, and the exchange-striction coefficients α_n, shown in Table 1 of the main text, were obtained by a least-square fit of Eq. 2 to the DFT results.

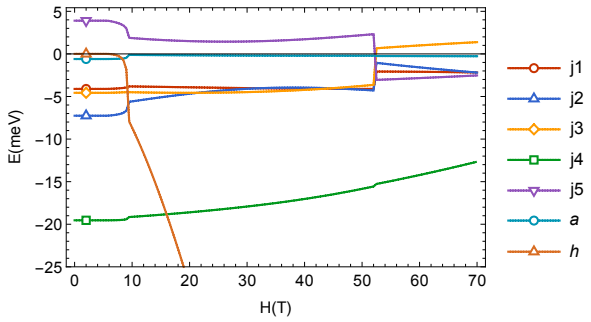

FIG. S4. Contributions to the total energy from different exchanges $J_1 \dots J_5$, single-ion anisotropy (marked a) and Zeeman energy (marked h), calculated using the model Eq. 1 of the main text, as functions of the applied magnetic field H_c.

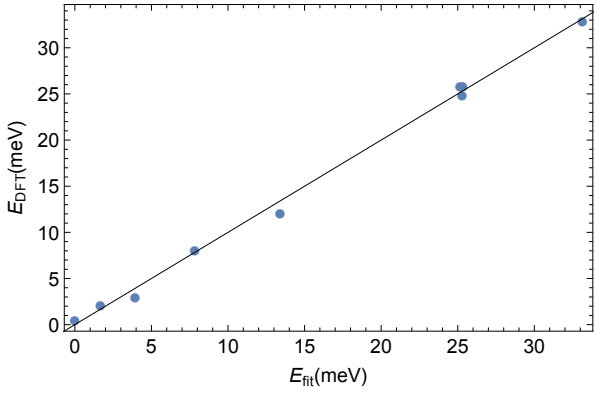

FIG. S5. The energies of trial magnetic states calculated using PBE0 and from the fit Eq. 1.

[1] Y. S. Oh, S. Artyukhin, J. J. Yang, V. Zapf, J. W. Kim, D. Vanderbilt, and S.-W. Cheong, Nat. Commun. **5**, 3201 (2014).

[2] J. A. Detwiler, G. M. Schmiedeshoff, N. Harrison, A. H. Lacerda, J. C. Cooley, and J. L. Smith, Phys. Rev. B **61**, 402 (2000).

[3] R. Daou, F. Weickert, M. Nicklas, F. Steglich, A. Haase, and M. Doerr, Rev. Sci. Inst. **81**, 033909 (2010).

[4] G. M. Schmiedeshoff, A. W. Lounsbury, D. J. Luna, S. J. Tracy, A. J. Schramm, S. W. Tozer, V. F. Correa, S. T. Hannahs, T. P. Murphy, E. C. Palm, A. H. Lacerda, S. L. Budko, P. C. Canfield, J. L. Smith, J. C. Lashley, and J. C. Cooley, Rev. Sci. Instrum. **77**, 123907 (2006).

[5] J. W. Kim, Y. Kamiya, E. D. Mun, M. Jaime, N. Harrison, J. D. Thompson, V. Kiryukhin, H. T. Yi, Y. S. Oh, S.-W. Cheong, C. D. Batista, and V. S. Zapf, Phys. Rev. B **89**, 060404(R) (2014).

[6] V. S. Zapf, M. Kenzelmann, F. Wolff-Fabris, F. Balakirev, and

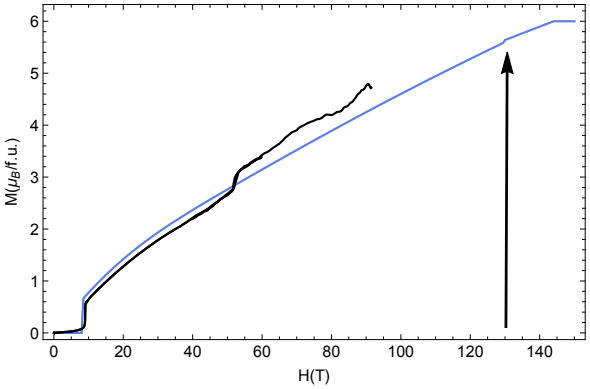

FIG. S6. The magnetization $M_c(H_c)$ under the applied magnetic field H_c, calculated using the model Eq. 1 of the main text, PBE0 exchange constants and $A = 0.05$ meV (blue line), and measured in the experiment (black line). The second transition obtained from the model calculations is indicated by the black arrow.

Y. Chen, Phys. Rev. B **82**, 060402 (2010).

[7] S. H. Chun, Y. S. Chai, Y. S. Oh, D. Jaiswal-Nagar, S. Y. Haam, I. Kim, B. Lee, D. H. Nam, K.-T. Ko, J. H. Park, J.-H. Chung, and K. H. Kim, Phys. Rev. Lett. **104**, 037204 (2010).

[8] N. Lee, C. Vecchini, Y. J. Choi, L. C. Chapon, A. Bombardi, P. G. Radaelli, and S.-W. Cheong, Phys. Rev. Lett. **110**, 137203 (2013).

[9] T. Aoyama, K. Yamauchi, A. Iyama, S. Picozzi, K. Shimizu, and T. Kimura, Nat. Commun. **5**, 4927 (2014).

[10] F. Wu, E. Kan, C. Tian, and M.-H. Whangbo, Inorg. Chem. **49**, 7545 (2010).

[11] I. Živković, K. Prša, O. Zaharko, and H. Berger, J. Phys.: Condens. Matter **22**, 056002 (2010).

[12] X. Rocquefelte, K. Schwarz, and P. Blaha, Sci. Rep. **2**, 759 (2012).

[13] G. Kresse and J. Hafner, Phys. Rev. B **47**, 558 (1993).

[14] G. Kresse and J. Hafner, Phys. Rev. B **49**, 14251 (1994).

[15] P. E. Blochl, Phys. Rev. B **50**, 17953 (1994).

[16] G. Kresse and J. Furthmller, Comput. Mat. Sci. **6**, 15 (1996).

[17] G. Kresse and J. Furthmuller, Phys. Rev. B **54**, 11169 (1996).

[18] J. P. Perdew, K. Burke, and M. Ernzerhof, Phys. Rev. Lett. **77**, 3865 (1996).

[19] J. P. Perdew, K. Burke, and M. Ernzerhof, Phys. Rev. Lett. **78**, 1396 (1997).

[20] G. Kresse and D. Joubert, Phys. Rev. B **59**, 1758 (1999).

[21] C. Adamo and V. Barone, J. Chem. Phys. **110**, 6158 (1999).